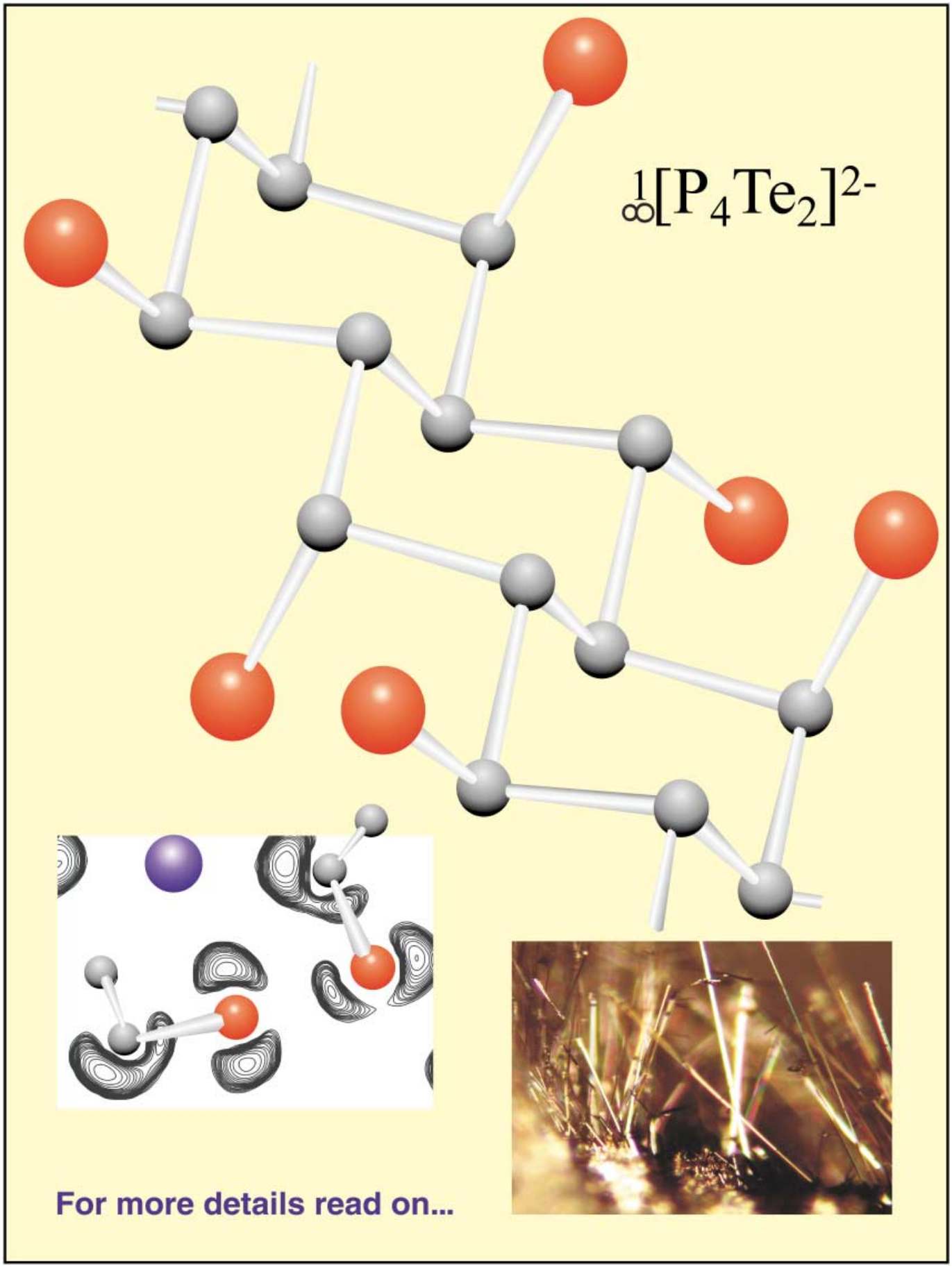

 DOI: 10.1002/chem.200304858

BaP_4Te_2—A Ternary Telluride with P–Te Bonds and a Structural Fragment of Black Phosphorus

Stefan Jörgens,[a] Dirk Johrendt,[b] and Albrecht Mewis*[a]

Abstract: The new telluride BaP_4Te_2 was synthesized in form of gleaming black needles by heating stochiometric mixtures of the elements to 475 °C for 100 h. The crystal structure was determined by single-crystal X-ray methods. BaP_4Te_2 crystallizes orthorhombically, space group *Pnma* with $a = 16.486(8)$, $b = 6.484(2)$, $c = 7.076(4)$ Å, and $Z = 4$. A main feature of the so far unknown crystal structure type are P_4Te_2 chains that consist of condensed six-membered rings of phosphorus. These strands are equivalent to a structural fragment of black phosphorus, in which each of the lateral atoms is connected to a tellurium atom. The chains running along [010] are separated from each other by barium atoms, that is, linked through Ba–Te and Ba–P bonds. BaP_4Te_2 is an electron precise compound according to the Zintl concept, and the formula can be split ionically as follows: $BaP_4Te_2 \equiv Ba^{2+}(P^0)_4(Te^-)_2$. The remarkable Te–P bonds have been analyzed by electronic structure calculations using the electron localization function (ELF) and the crystal orbital Hamiltonian population (COHP) methods.

Keywords: barium · chemical bonding · phosphorus · structure elucidation · tellurium · X-ray diffraction

Introduction

The reactivity of phosphorus to tellurium is very different by comparison to the other chalcogens. Due to the pronounced instability of P–Te bonds, no binary phosphorus tellurides exist so far apart from miscellaneous compounds such as P_4STe_2.[1] On the other hand, it is well known that the P–Te bond can be stabilized in organometallic compounds, for example, in trialkylphosphane tellurides such as $(iso\text{-}C_3H_7)_3PTe$.[2] In the field of intermetallic phases, two groups of compounds exist. For the first group, UPTe[3] is an example that crystallizes in the tetragonal La_2Sb type.[4] In this structure, there are U–P and U–Te bonds, but no interactions between phosphorus and tellurium. The shortest P–Te distance is 3.84 Å and therefore too long with regard to the sum of the covalent radii (2.47 Å[5]). IrPTe[6] and OsPTe[7], for example, belong to the second group of intermetallic phases. They are structurally related to pyrites and marcasites, but with lower symmetry due to the replacement of the symmetrical S_2 group by PTe. Their crystal structures, based on powder diffraction data, are not reliably known, but P–Te bonds therein are probable from spectroscopic data. Because of the evident weakness of P–Te bonds, the situation is similar in the field of chalcogenophosphates. A large number of thio- and selenophosphates exist, for example, A_2AuPS_4, $A_3AuP_2Se_8$ (A = K, Rb, Cs)[8] or $K_3La(PS_4)_2$[9], but no homologous tellurophosphates are known up to now. Our attempts to synthesize such compounds resulted in the novel phosphorus–telluride BaP_4Te_2. In this paper we report its preparation, crystal structure, and chemical bonding.

[a] Prof. Dr. A. Mewis, S. Jörgens
Institut für Anorganische Chemie und
Strukturchemie II der Heinrich-Heine-Universität
Universitätsstrasse 1
40225 Düsseldorf (Germany)
Fax: (+49) 211-81-14146
E-mail: albrecht.mewis@uni-duesseldorf.de

[b] Prof. Dr. D. Johrendt
Department Chemie
Ludwig-Maximilians-Universität München
Butenandtstrasse 5–13 (Haus D)
81377 München (Germany)
Fax: (+49) 89-2180-77430
E-mail: dirk.johrendt@cup.uni-muenchen.de

Results and Discussion

BaP_4Te_2 crystallizes in a new orthorhombic structure type with four formula units per unit cell. The structure is shown in Figure 1; selected bond lengths and angles are summarized in Table 1.

The main features of the crystal structure of BaP_4Te_2 are the existence of short P–Te bonds and six-membered rings of phosphorus in a chair form; these rings are condensed by the P2 atoms as illustrated in Figure 2. These one-dimensional bands along [010] correspond to a fragment of black phosphorus or gray arsenic. The P2 atoms are involved in three homonuclear bonds, whereas each of the other P atoms

  DOI: 10.1002/chem.200304858

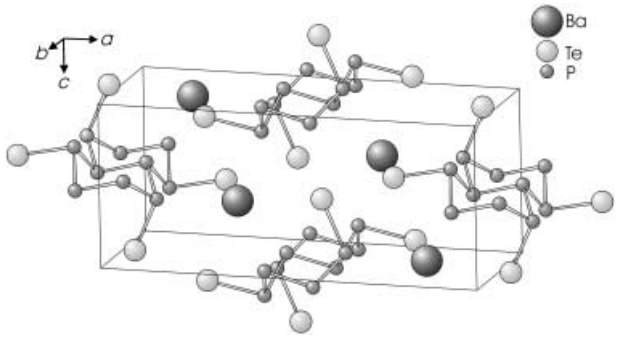

Figure 1. Crystal structure of BaP_4Te_2.

Table 1. Selected bond lengths [Å] and angles [°] for BaP_4Te_2.

Ba–P3	3.258(6)	P2-P1-P2	97.7(7)
Ba–P2	3.397(3) 2 ×	P2-P1-Te2	106.9(2)
Ba–Te1	3.575(1) 2 ×	P2-P2-P1	104.5(2)
Ba–Te2	3.699(2)	P3-P2-P1	96.1(2)
P1–P2	2.221(4) 2 ×	P3-P2-P2	95.1(2)
P1–Te2	2.469(6)	P2-P3-P2	90.9(3)
P2–P3	2.203(5)	P2-P3-Te1	95.3(2)
P2–P2	2.213(6)		
P3–Te1	2.537(5)		

is connected to one tellurium atom as a third neighbor. The two Te atoms per six-membered ring occupy axial as well as equatorial positions. The P–P bond lengths extend from 2.20 to 2.22 Å, in agreement with those of black phosphorus.[10] The same is true for the bond angles ranging from 90.9 to 104.5° (black phosphorus: 96.3 and 102.1°). The P–Te distances of 2.47 Å and 2.54 Å, respectively, are in the range of the sum of the covalent radii (2.47 Å)[5], indicating the presence of covalent P–Te bonding.

The phosphorus atoms are threefold connected in the one-dimensional P_4Te_2 bands, and have the formal charge ±0, whereas the terminal tellurium is −1. Certainly there is an electron transfer from barium to the $[P_4Te_2]^{2-}$ unit, and, therefore, BaP_4Te_2 is a valence compound in a classical view and it belongs to the Zintl phases in a broader sense. As shown in Figure 3, the coordination polyhedron around barium is irregular and consists of three P and Te atoms each that belong to several P_4Te_2 bands. Additional atoms (1 P, 4 Te) complete the polyhedron at distances exceeding the sums of radii by more than 5% (Ba: atomic radius (coordination number: 12); P, Te: covalent radius).

Abstract in German: *Das neue Tellurid BaP_4Te_2 wurde durch Erhitzen eines der Formel entsprechenden Elementgemenges auf 475 °C dargestellt und dabei in Form metallisch glänzender schwarzer Nadeln erhalten. Die Bestimmung der Kristallstruktur erfolgte röntgenographisch auf der Basis von Einkristalldaten und ergab orthorhombische Symmetrie (Pnma; a = 16.486(8), b = 6.484(2), c = 7.076(4) Å; Z = 4). Hervorstechendes Strukturmerkmal sind P_4Te_2-Ketten aus miteinander verknüpften sechsgliedrigen Phorphor-Ringen in Sessel-Konformation. Sie stellen damit ein Fragment der Struktur des schwarzen Phosphors dar, bei dem die seitlichen P-Atome jeweils mit einem Te-Atom verbunden sind. Die Ketten verlaufen entlang [0 1 0] und werden durch Ba-Atome voneinander getrennt, mit denen sie über Ba–Te- sowie Ba–P-Bindungen Kontakt haben. Folgt man dem Zintl-Konzept, ist BaP_4Te_2 entsprechend der ionischen Formulierung $Ba^{2+}(P^0)_4(Te^-)_2$ elektrovalent aufgebaut. Die elektronische Struktur sowie die Bindungsverhältnisse insbesondere der Te–P Bindung werden mit der Elektronenlokalisierungsfunktion (ELF) und der COHP Methode diskutiert.*

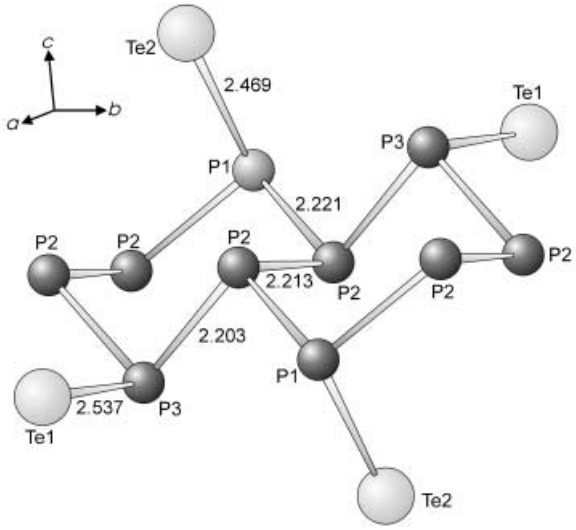

Figure 2. Cutout of the $^1_\infty[P_4Te_2]^{2-}$ chain of BaP_4Te_2.

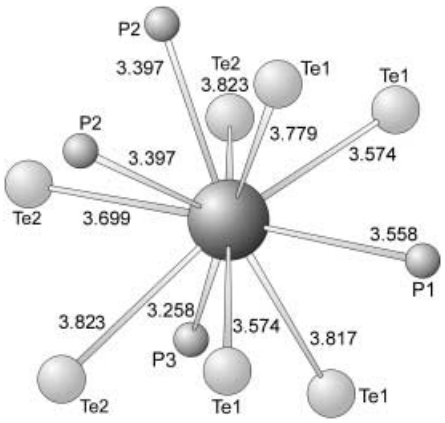

Figure 3. Coordination of barium in BaP_4Te_2.

Compounds with structural fragments of black phosphorus are well known in numerous AP_3 polyphosphides with A = Ca, Sr, Ba. Their structures are formed by disintegration of the two-dimensional network of phosphorus, that is, removing atoms in different ways. In BaP_3, for example, only neighboring atoms are removed, and a one-dimensional structure is formed built up of infinitely connected six-membered rings with chair form and axial linkage.[11] In SrP_3[12] half of the P rings remain complete, whereas in CaP_3[13] all of them are opened. A very similar arrangement as found in BaP_4Te_2 exists in the structure of LiP_5.[14] Figure 4 shows one-dimensional bands of condensed six-membered P rings running along [0 0 1]. Instead of tellurium they are connected by P atoms that

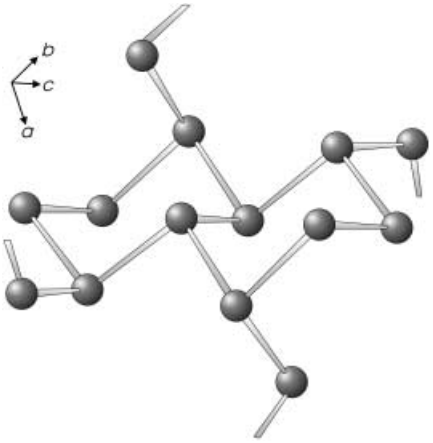

Figure 4. Cutout of the anionic network of LiP_5.

occupy axial as well as equatorial positions. In contrast to BaP_4Te_2 each of these atoms is part of two bands forming a three-dimensional network. Just as tellurium in BaP_4Te_2, the twofold-linked P atoms have the formal charge -1, which is compensated by the electropositive metal lithium.

To our knowledge, BaP_4Te_2 is the first structurally characterized ternary compound to contain P–Te bonds that are not stabilized by organometallic ligands. We had no success in synthesizing other compounds of the formula AP_4Te_2 with A = Ca, Sr, and Sn, mainly resulting in binary ATe. Comparable results were obtained from our attempts to prepare BaP_4Se_2 and BaP_4S_2; these yielded BaSe, BaS, or $Ba_2P_2S_6$.[15]

According to the above-mentioned formula splitting $Ba^{2+}(P^0)_4(Te^-)_2$, all valence electrons should be localized in covalent bonds or lone pairs. Therefore, BaP_4Te_2 is expected to be an insulator or semiconductor. To check this and to support the interpretation of chemical bonding derived from interatomic distances, we have calculated the electronic structure as well as the electron localization function of BaP_4Te_2. From the viewpoint of chemical bonding, the P–Te bond is the most striking feature, and, therefore, our electronic structure analysis is focused mainly on it.

Figure 5 shows the total density of states (DOS) and the contributions of the Te and P atoms. A band gap of $\sim$1.3 eV is observed above the Fermi level, in agreement with the proposed semiconducting property. The total DOS (dotted line in Figure 5) splits roughly into two parts. The s states of tellurium and phosphorus extend from -15 to -7 eV, followed by the range of p levels from -7 eV to the Fermi energy. It is worth noting the differences in the distributions of the P 3p and Te 5p states between -7 and 0 eV, which are larger as expected from electronegativity reasons (P: 2.1 and Te 2.0). Most of the Te 5p states are in the large peak between -2 and 0 eV (solid line in Figure 5), in which only a small amount of P 3p levels occurs. The main part of P 3p states is between -7 and -2 eV (dashed line in Figure 5), over which the Te contribution is rather small. However, this is exactly the energy range of the P–Te ppσ-bonding states, as seen from the crystal orbital Hamiltonian population (COHP) diagram of the P–Te bond in Figure 6. In contrast to this, the range from -2 to 0 eV is weakly P–Te antibonding, and the explanation for this is a weak π-type interaction between phosphorus and tellurium, which gives rise to only a small splitting between the fully occupied ppπ- and ppπ* levels. This is in agreement with a simple molecular orbital scheme of a diatomic PTe^- fragment: 12 electrons fill exactly the ssσ, ppσ, $2\times$ ppπ and $2\times$ ppπ* orbitals.

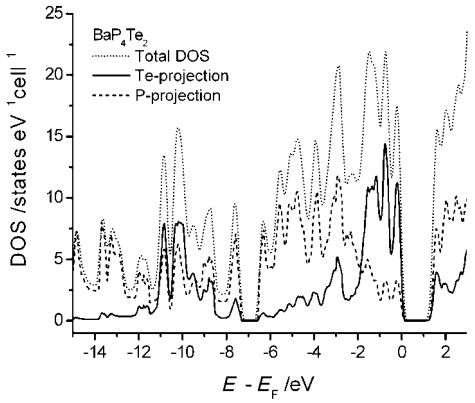

Figure 5. Total and projected density of states of BaP_4Te_2.

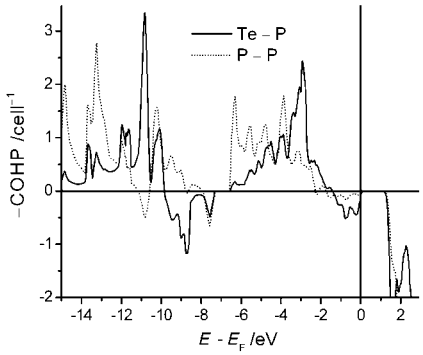

Figure 6. COHP diagrams of the Te–P and P–P bonds in BaP_4Te_2.

What we can extract from the DOS and COHP diagrams is the existence of a covalent P–Te bond and distinct lone pairs located at the Te atoms. The homonuclear P–P bonds occur in the COHP as expected. These results clearly support the $Ba^{2+}(P^0)_4(Te^{1-})_2$ formula splitting. The bonding picture is further visualized by the electron localization function (ELF), shown in Figure 7. The xz plane at $y = ¼$ contains the P–Te bonds of interest, and the areas with high ELF values are absolutely consistent with the picture drawn from the DOS and COHP. Large lone pairs surround the Te atoms and occur at the P atoms on top of the $(P2)_2P1$-Te pyramid, as expected for phosphorus in the oxidation state zero. The covalent P–Te bonds are also clearly visible by the area of high ELF lying on the bond axis. This covalent attraction is remarkably shifted to the phosphorus atom, taking the higher electronegativity into account.

Experimental Section

Synthesis and X-ray investigations: A stoichiometric mixture of Ba (0.103 g, 0.75 mmol), P (0.093 g, 3.003 mmol), and Te (0.191 g, 1.497 mmol)

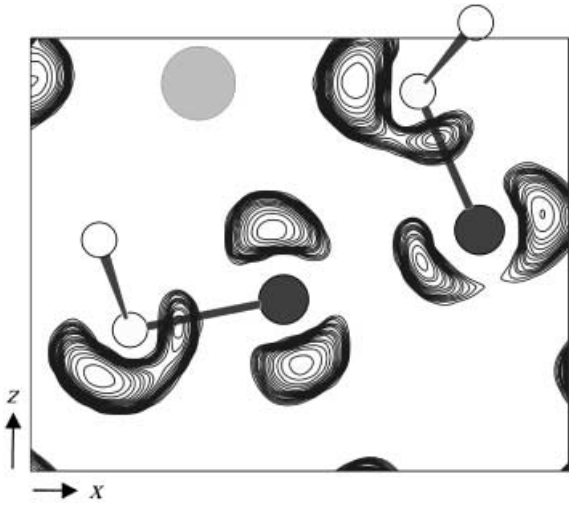

Figure 7. Electron localisation function ELF of BaP_4Te_2 within the xz plane at $y = ¼$ The contour lines range from ELF = 0.8 to 0.96. White circles: P atoms, dark grey: Te atoms, light grey: Ba atoms.

was loaded into a silica tube, which was sealed under vacuum. The mixture was heated at a rate of 30 °C h^{-1} up to 475 °C, kept at this temperature for 100 h, and cooled down in the furnace to room temperature. This yielded gleaming black crystals (needles) and powder of BaP_4Te_2, stable in air for weeks. Single crystals suitable for X-ray experiments were selected directly from the reaction product. No impurities could be detected within the accuracy of the X-ray powder diffraction experiment (Huber G 600, Cu$K_{\alpha 1}$, calibrated with Si). The energy-dispersive X-ray (EDX) analysis (DS 130 ISI, EDAX-DX4) of selected crystals was in good agreement with the expected composition. Single-crystal intensity data were collected at room temperature by use of a four-circle diffractometer (P3). Scans were taken in the $\omega/2\theta$ mode; an empirical absorption correction was applied on the basis of ψ-scan data. The structure was solved in the centrosymmetric space group *Pnma* by direct methods and refined against F^2 (SHELXL-97).[16] Crystallographic data and details of the data collection are given in Table 2; the final atomic and equivalent displacement parameters are listed in Table 3. Selected bond lengths and angles are summarized in Table 1. Further details of the crystal structure investigation can be obtained from the Fachinformationszentrum Karlsruhe, 76344 Eggenstein-Leopoldshafen, Germany, (fax: (+49)7247–808–666; e-mail: crysdata@fiz.karlsruhe.de) on quoting the depository number CSD-412643.

Table 2. Crystallographic data and details of the data collection for BaP_4Te_2.

crystal system	orthorhombic
space group	*Pnma*
a [Å]	16.486(8)
b [Å]	6.484(2)
c [Å]	7.076(4)
V [Å^3]	756.4(6)
Z	4
ρ_{calcd} [g cm^{-3}]	4.535
μ [mm^{-1}]	13.54
min/max transmission	0.680/0.956
2θ range [°]	3–67
index range (hkl)	0, +25; ±10; 0, +11
reflections collected	2976
unique reflections	1597
observed reflections [$I > 2\sigma(I)$]	683
parameters	41
R_1 [$I > 2\sigma(I)$]	0.051
wR_2 (all data)	0.114
goodness-of-fit	0.714
residual electron density [e Å^{-3}]	1.93/0.96

Table 3. Atomic coordinates and equivalent displacement parameters [pm^2][a] for BaP_4Te_2.

Atom	Position	x	y	z	U_{eq}
Ba	4*c*	0.1625(1)	¼	0.1015(2)	168(3)
P1	4*c*	0.3781(3)	¼	0.1200(7)	127(9)
P2	8*d*	0.0650(2)	0.0079(5)	0.4616(4)	130(6)
P3	4*c*	0.0953(3)	¼	0.6684(8)	162(11)
Te1	4*c*	0.2462(1)	¼	0.5986(2)	161(3)
Te2	4*c*	0.4388(1)	¼	0.4390(2)	172(3)

[a] The equivalent displacement parameter is defined as one-third of the orthogonalized U_{ij} tensor.

Electronic structure calculations: Self-consistent ab initio band structure calculations were performed with the LMTO method in its scalar relativistic version (program LMTO-ASA 47).[17] A detailed description may be found elsewhere.[18–22] Reciprocal space integrations were performed with the tetrahedron method by using 1138 irreducible k-points within the Brillouin zone.[23] The basis sets consisted of 6s/5d/4f for Ba, 3s/3p for P, and 5s/5p for Te. The 6p orbitals of Ba, 5d/4f of Te, and 3d of P were treated by the downfolding technique.[24] To achieve space filling within the atomic sphere approximation, interstitial spheres were introduced to avoid too large overlap of the atom centered spheres. The empty sphere positions and radii were calculated by using an automatic procedure developed by Krier.[25] We did not allow an overlap of more than 15 % for any two atom-centered spheres. Two-dimensional grids of the electron localization function (ELF)[26] were calculated. Within density functional theory, ELF depends on the excess of local kinetic energy owing to the Pauli principle compared with the bosonic system (Pauli kinetic energy $t_{P(r)}$). By definition the values for ELF are confined to the range 0–1. Regions in space for which the Pauli principle does not increase the kinetic energy of the electrons (i.e. , high values of ELF) can be identified as areas in which pairing of electrons with opposite spins play an important role. Thus, high values of ELF can be treated as equivalent to covalent bonds or lone pairs.[27] The crystal orbital Hamiltonian population (COHP) method was used for the bond analysis.[28] COHP gives the energy contributions of all electronic states for a selected bond. The values are negative for bonding and positive for antibonding states. With respect to the well-known COOP diagrams, we plotted −COHP(E) to obtain positive values for bonding states.

Acknowledgement

The support of this work by the Fonds der Chemischen Industrie is gratefully acknowledged.

[1] H. P. Baldus, R. Blachnik, *Z. Naturforsch. Teil B* **1990**, *45*, 1605.
[2] N. Kuhn, G. Henkel, H. Schumann, R. Fröhlich, *Z. Naturforsch. Teil B* **1990**, *45*, 1010.
[3] A. Zygmunt, A. Murasik, S. Ligenza, J. Leciejewicz, *Phys. Status. Solidi A* **1974**, *22*, 75.
[4] W. N. Stassen, M. Sato, L. D. Calvert, *Acta Crystallogr. Sect. B* **1970**, *26*, 1534.
[5] L. Pauling, *Die Natur der Chemischen Bindung*, 3rd ed., VCH, Weinheim, **1968**, p. 379.
[6] G. Kliche, *Z. Naturforsch. Teil B* **1986**, *41*, 130.
[7] H. D. Lutz, T. Schmidt, G. Wäschenbach, *Z. Anorg. Allg. Chem.* **1988**, *562*, 7.
[8] K. Chondroudis, J. A. Hanko, M. G. Kanatzidis, *Inorg. Chem.* **1997**, *36*, 2623, and references therein.
[9] C. R. Evenson IV, P. K. Dorhout, *Inorg. Chem.* **2001**, *40*, 2884, and references therein.
[10] A. Brown, S. Rundqvist, *Acta Crystallogr.* **1965**, *19*, 684.
[11] H. G. von Schnering, W. Dahlmann, *Naturwissenschaften* **1971**, *58*, 623.

[12] W. Dahlmann, H. G. von Schnering, *Naturwissenschaften* **1973**, *60*, 429.
[13] W. Dahlmann, H. G. von Schnering, *Naturwissenschaften* **1973**, *60*, 518.
[14] H. G. von Schnering, W. Wichelhaus, *Naturwissenschaften* **1972**, *59*, 78; J. Schmedt a. d. Günne, S. Kaczmarek, L. v. Wüllen, H. Eckert, D. Paschke, A. J. Foecker, W. Jeitschko, *J. Solid State Chem.* **1999**, *147*, 341.
[15] S. Jörgens, A. Mewis, R.-D. Hoffmann, R. Pöttgen, B. D. Mosel, *Z. Anorg. Allg. Chem.* **2003**, *629*, 429.
[16] G. M. Sheldrick, SHELXL-97, Universität Göttingen, **1997**.
[17] O. K. Andersen, Tight-Binding LMTO Vers. 47, Max-Planck-Institut für Festkörperforschung, Stuttgart, **1994**.
[18] O. K. Andersen, *Phys. Rev.* **1975**, *B12*, 3060.
[19] O. Jepsen, O. K. Andersen, *Phys. Rev. Lett*. **1984**, *53*, 2571.
[20] O. K. Andersen, O. Jepsen, *Z. Phys.* **1995**, *B97*, 35.
[21] H. L. Skriver, *The LMTO Method*, Springer, Berlin, **1984**.
[22] O. Jepsen, M. Snob, O. K. Andersen, *Linearized Band-Structure Methods in Electronic Band-Structure and its Applications*, Springer, Lecture Notes, Springer, Berlin, **1987**.
[23] O. K. Andersen, O. Jepsen, *Solid State Commun*. **1971**, *9*, 1763.
[24] W. R. L. Lambrecht, O. K. Andersen, *Phys. Rev. B* **1986**, *34*, 2439.
[25] G. Krier, O. Jepsen, O. K. Andersen, unpublished results.
[26] A. Savin, B. Silvi, *Nature* **1994**, *371*, 683.
[27] A. Savin, T. F. Fässler, *Chem. Unserer Zeit* **1997**, *31*, 110.
[28] R. Dronskowski, P.Blöchl, *J. Phys. Chem*. **1993**, *97*, 8617.

Received: February 18, 2003 [F4858]